

Critical scaling near the yielding transition in granular media

Abram H. Clark,^{1,2} Jacob D. Thompson,¹ Mark D. Shattuck,³ Nicholas T. Ouellette,⁴ and Corey S. O'Hern^{2,5,6}

¹*Department of Physics, Naval Postgraduate School, Monterey, California 93943, USA*

²*Department of Mechanical Engineering and Materials Science,*

Yale University, New Haven, Connecticut 06520, USA

³*Benjamin Levich Institute and Physics Department,*

The City College of the City University of New York, New York, New York 10031, USA

⁴*Department of Civil and Environmental Engineering,
Stanford University, Stanford, California 94305, USA*

⁵*Department of Physics, Yale University, New Haven, Connecticut 06520, USA*

⁶*Department of Applied Physics, Yale University, New Haven, Connecticut 06520, USA*

(Dated: December 14, 2024)

We show that the yielding transition in granular media displays second-order critical-point scaling behavior. We carry out discrete element simulations in the low inertial number limit for frictionless, purely repulsive spherical grains undergoing simple shear at fixed nondimensional shear stress Σ in two and three spatial dimensions. To find a mechanically stable (MS) packing that can support the applied Σ , isotropically prepared states with size L must undergo a total strain $\gamma_{\text{ms}}(\Sigma, L)$. The number density of MS packings ($\propto \gamma_{\text{ms}}^{-1}$) vanishes for $\Sigma > \Sigma_c \approx 0.11$ according to a critical scaling form with a length scale $\xi \propto |\Sigma - \Sigma_c|^{-\nu}$, where $\nu \approx 1.8$. Above the yield stress ($\Sigma > \Sigma_c$), no MS packings that can support Σ exist in the large system limit, $L/\xi \gg 1$. MS packings generated via shear possess anisotropic force and contact networks, suggesting that Σ_c is associated with an upper limit in the degree to which these networks can be deformed away from those for isotropic packings.

Granular materials consist of macroscopic grains that interact via dissipative contact forces. Their response to external forcing depends on the ratio $\Sigma = \tau/p$ of the applied shear stress τ to the normal stress p , where p is small compared to the stiffness of the grains [1, 2]. Granular media, like other amorphous materials [3–6], possess a yield stress Σ_c . When $\Sigma < \Sigma_c$, grains move temporarily until finding a solid-like mechanically stable (MS) packing that can support the applied Σ [7–9]. When $\Sigma = \Sigma_c$, the strain γ_{ms} required to find MS packings diverges. When $\Sigma > \Sigma_c$, grains cannot find MS packings, and fluid-like flow persists indefinitely.

In the jamming scenario [10–16], the packing fraction ϕ is the controlling variable. Fluid- and solid-like states occur for $\phi < \phi_J$ and $\phi > \phi_J$, respectively. A diverging length scale $\xi_J \propto |\phi - \phi_J|^{-\nu_J}$ controls the mechanical response near ϕ_J [12, 14–16]. However, MS packings of frictionless grains at fixed p and varied Σ all have a packing fraction $\phi_{\text{ms}}(\Sigma) \approx \phi_J$ [9]. Thus, the behavior for $\Sigma \approx \Sigma_c$ may represent a fluid-solid transition distinct from jamming, where the structure of the force and contact networks, not ϕ , plays a dominant role.

In this Letter, we show evidence that the number density of MS packings vanishes at $\Sigma = \Sigma_c$ in the large-system limit, with second-order critical scaling related to the structure of the force and contact networks, and not ϕ . We measure γ_{ms} in systems of frictionless grains subjected to simple shear as a function of Σ and system size L . We postulate a second-order critical point scaling form for γ_{ms} with a diverging length scale $\xi \propto |\Sigma - \Sigma_c|^{-\nu}$. The data for γ_{ms} collapse onto two branches: $\Sigma > \Sigma_c$ and $\Sigma < \Sigma_c$, with $\Sigma_c \approx 0.11$ for simple shear in two- (2D) and three-dimensions (3D). MS packings exist for

$\Sigma > \Sigma_c$ in small systems, but the number vanishes as L/ξ increases. For $\Sigma < \Sigma_c$, MS packings exist for all L , and large systems ($L > \xi$) are equivalent to compositions of uncorrelated smaller systems.

Our results are insensitive to changes in the boundary conditions and driving method, which we explicitly show by performing additional simulations in a riverbed-like geometry in the viscous limit [17, 18]. We find that the packing fraction $\phi_{\text{ms}}(\Sigma, L)$ of MS packings is independent of Σ , but the anisotropy in both the stress and contact fabric tensors of MS packings increases with Σ , suggesting that Σ_c is associated with an upper limit to the structural anisotropy that can be realized in the large-system limit [9]. These results may help explain recent studies [19–23] showing that accurately modeling granular flows requires a cooperative length scale that grows as a power law in $\Sigma - \Sigma_c$. Our results may also be relevant to other amorphous solids that show similar spatial cooperativity near yielding [5, 24–26].

We perform discrete element method simulations of simple shear in 2D and 3D, as well as a 2D riverbed-like geometry subjected to a linear flow profile in the viscous limit. We study systems of bidisperse frictionless spheres in 3D and disks in 2D. Two-thirds of grains are small and one-third are large, with diameter ratio 1.2 in 3D and 1.4 in 2D. We begin with 3D simple shear, as depicted in Fig. 1 (a). The lateral directions x and z are periodic with length L , where L is the length of the box edge in units of the small grain diameter D . The lower y boundary consists of a no-slip wall. The system is driven by the upper boundary, which is a plate consisting of rigidly connected small particles, with gaps that are large enough to prevent slip and small enough to stop bulk particles from

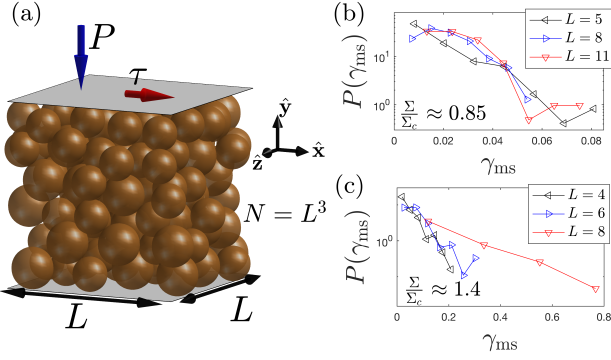


FIG. 1. (a) A schematic of the simulation procedure with the x -, y -, and z -directions indicated. MS packings are first created under only a fixed normal force per area $-p\hat{y}$. We then apply a shear force per area $\tau\hat{x}$ and search for an MS packing at a given $\Sigma = \tau/p$ and length L in units of the small grain diameter D . (b-c) Distributions $P(\gamma_{\text{ms}})$ of the strain γ_{ms} between the initial and final MS packings for (b) $\Sigma < \Sigma_c$, (c) $\Sigma > \Sigma_c$, and several L .

passing through the plate. Our results are insensitive to the details of the top plate, provided no slip occurs between the plate and grains. We apply downward force per area $-p\hat{y}$ and horizontal force per area $\tau\hat{x}$ to the upper plate and solve Newton's equations of motion for the wall as well as $N = L^3$ grains (from $L = 3$, $N = 27$ to $L = 12$, $N = 1728$) using a modified velocity Verlet integration scheme. Particles interact via purely repulsive, linear springs with force constant K . We include a viscous damping force $-B\mathbf{v}$ in the equations of motion for the top plate and N grains, where \mathbf{v} is the absolute velocity and B is the damping coefficient.

The equations of motion for simple shear, described in detail in the Supplemental Material, are governed the nondimensional parameters $\kappa = \frac{K}{pD^{d-1}}$, $\Gamma = \frac{B}{\sqrt{mpD^{d-2}}}$, and $\Sigma = \frac{\tau}{p}$, where d is the spatial dimension. We set $\kappa = 10^3$, meaning that $\phi \approx \phi_J(L) + 0.001$, where $\phi_J(L)$ is the jamming packing fraction at a given L . Our results are insensitive to κ in this limit, which we verify for several values of $\kappa > 200$. We set $\Gamma = 5$, which maintains an inertial number $I = \dot{\gamma}\sqrt{m/p} < 10^{-4}$ (where $\dot{\gamma}$ is the strain rate) in the slow- or creep-flow limit, $I < 10^{-3}$ [1, 19]. We control force and not $\dot{\gamma}$, so there are fluctuations in I , but $\Gamma = 5$ keeps $I < 10^{-4}$ even for $\Sigma > \Sigma_c$. We show in Supplemental Material that our results are independent of Γ for $\Gamma = 3, 5$, and 7 .

Initial states ($\Sigma = 0$) are prepared via uniaxial compression by the top plate, which can shift laterally until an MS packing is found. We then apply finite Σ to the top plate, which can move in all directions. The simulation ends when the upward and horizontal forces from the grains acting on the top plate exactly balance the applied Σ . We find similar results when Σ is increased incrementally in small steps, and the total strain is inte-

grated. Average particle displacement profiles are linear, as expected [8, 27]. The ensemble-averaged packing fraction ϕ_{ms} of MS packings is independent of Σ , as shown in Supplemental Material.

We define the shear strain γ_{ms} as the total distance the top plate moves in the x -direction divided by the average of the initial and final y -positions of the top plate. In Fig. 1(b) and (c), we show the distribution $P(\gamma_{\text{ms}})$ for two illustrative values of Σ over a range of system sizes L , obtained using 200 simulations for each L . For small L above and below Σ_c , the distributions are roughly exponential, $P(\gamma_{\text{ms}}) \approx \langle \gamma_{\text{ms}} \rangle^{-1} \exp(-\gamma_{\text{ms}}/\langle \gamma_{\text{ms}} \rangle)$. This form indicates an underlying physical process resembling absorption [28], where the mean “travel distance” $\langle \gamma_{\text{ms}}(\Sigma, L) \rangle$ is inversely proportional to the density of absorbing MS packings as the system is sheared.

In Fig. 2 (a), we plot $\langle \gamma_{\text{ms}} \rangle$ versus L over a range of Σ . Figure 2 (b) shows that these data can be collapsed by plotting the scaled variables $L^{-1}/|\Sigma - \Sigma_c|^\nu$ and $\langle \gamma_{\text{ms}} \rangle^{-1}/|\Sigma - \Sigma_c|^\beta$, suggesting that finite size effects for $\langle \gamma_{\text{ms}}(\Sigma, L) \rangle^{-1}$ depend on a diverging correlation length $\xi \propto |\Sigma - \Sigma_c|^{-\nu}$,

$$\langle \gamma_{\text{ms}}(\Sigma, L) \rangle^{-1} = |\Sigma - \Sigma_c|^\beta f_{\pm} \left(\frac{L^{-1}}{|\Sigma - \Sigma_c|^\nu} \right). \quad (1)$$

f_{\pm} are the critical scaling functions for $\Sigma > \Sigma_c$ and $\Sigma < \Sigma_c$, respectively. Note that all quantities in Eq. (1) are dimensionless. As shown in Supplemental Material, we determine the critical values by fitting the data to this functional form, where the critical values are fit parameters. We systematically exclude small system sizes and large deviations $|\Sigma - \Sigma_c|$. We quantify the fits using reduced chi-squared, $\chi^2 = \sum_i (\Delta_i)^2/e_i^2$, where the sum is over all data points i shown in Fig. 2(a), Δ_i is the difference between the data and the fit, and e_i is the standard error in the mean (the standard deviation within that sample divided by the square root of the number of trials), represented as error bars in Fig. 2(a). We search for fits where $\chi^2/n \approx 1$ [16], where n is the number of data points minus the number of fit parameters, and the critical values are independent of the range of $|\Sigma - \Sigma_c|$. From this analysis, we estimate $\nu = 1.84 \pm 0.25$, $\Sigma_c = 0.11 \pm 0.01$, and $\beta/\nu = 0.57 \pm 0.05$. The uncertainty ranges represent one standard deviation. Despite the uncertainty, $\nu \approx 1.8$ for yielding appears distinct from $\nu_J \approx 0.6 - 1$ for jamming [10, 12, 16], suggesting that these are two separate, though possibly related, zero-temperature transitions.

For small $L^{-1}/|\Sigma - \Sigma_c|^\nu$ (i.e., $L > \xi$), f_{-} becomes constant, meaning that $\langle \gamma_{\text{ms}} \rangle^{-1} \propto |\Sigma - \Sigma_c|^\beta$ in the large-system limit for $\Sigma < \Sigma_c$. Also, a peak develops in $P(\gamma_{\text{ms}})$ at $\gamma_{\text{ms}} > 0$, as shown in Fig. 1(b). We interpret this behavior as spatial decorrelation, where large systems behave like compositions of uncorrelated exponentially distributed random variables, yielding a distribution that is peaked at $\gamma_{\text{ms}} > 0$ with a mean that is independent of

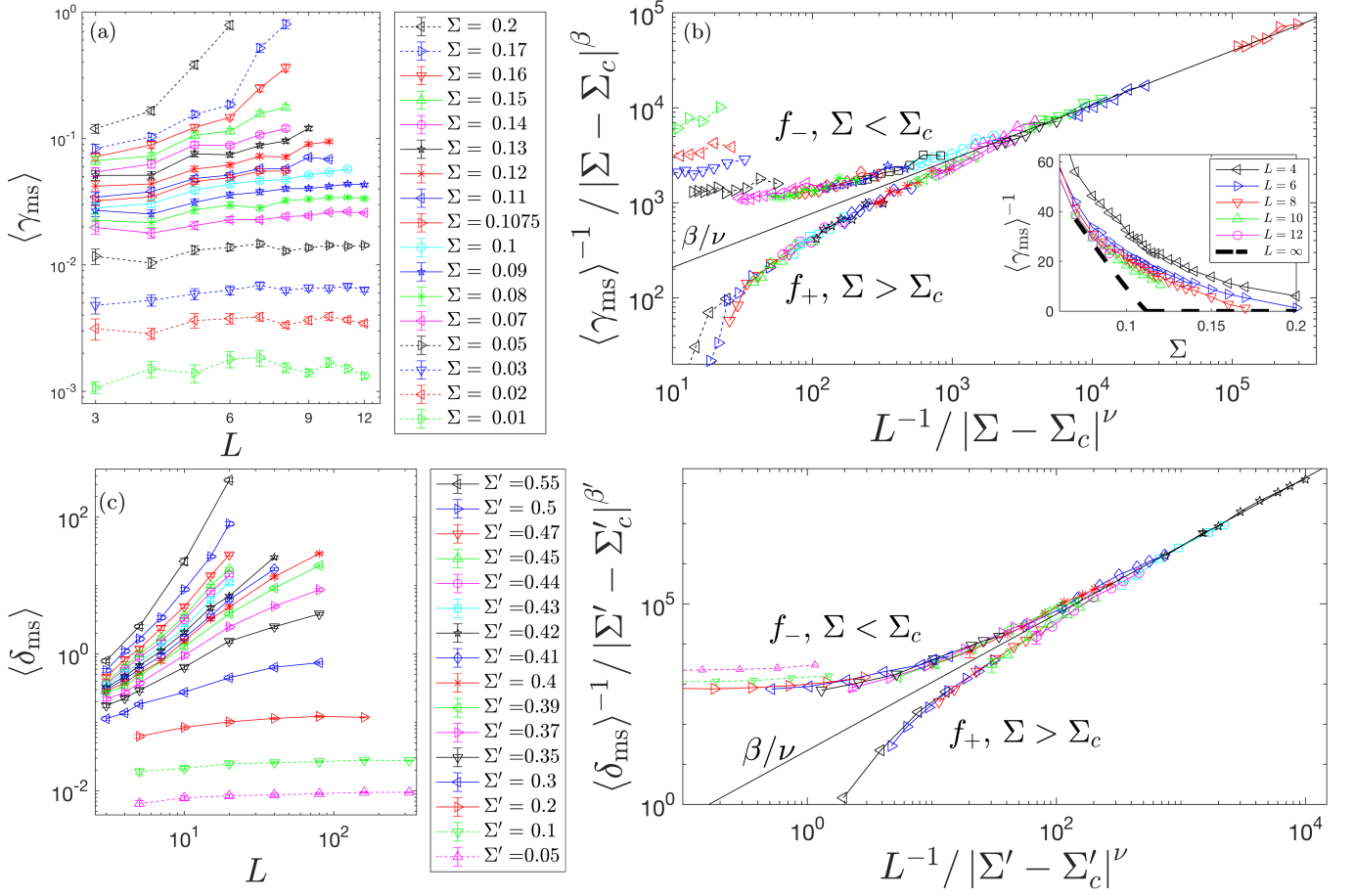


FIG. 2. (a) The mean strain $\langle \gamma_{\text{ms}} \rangle$ between initial and final MS packings plotted versus system size L for several values of applied stress Σ . Solid (dashed) lines correspond to $|\Sigma - \Sigma_c|/\Sigma_c$ less (greater) than 0.5. Error bars are the standard error of the mean, given by the standard deviation within the sample divided by the square root of the number of trials. (b) The data from panel (a), plus additional data for more Σ , collapses when using the scaled variables $\langle \gamma_{\text{ms}}(\Sigma, L) \rangle^{-1} / |\Sigma - \Sigma_c|^\beta$ and $L^{-1} / |\Sigma - \Sigma_c|^\nu$, where $\beta/\nu = 0.57$, $\nu = 1.8$, and $\Sigma_c = 0.108$. The inset shows $\langle \gamma_{\text{ms}}(\Sigma, L) \rangle^{-1}$ versus Σ for different L . The dashed line gives the large-system limit implied by Eq. (1) and the main plot in (b). (c) Analogous data to (a) for a riverbed-like geometry, showing the ensemble-averaged distance $\langle \delta_{\text{ms}} \rangle$ traveled by grains between initial and final MS packings at varying dimensionless shear force Σ' (see text for details). Solid (dashed) lines correspond to $|\Sigma' - \Sigma'_c|/\Sigma'_c$ less (greater) than 0.7 (d) Scaling collapse similar to (b) using $\Sigma'_c = 0.418$, $\nu = 1.8$, and $\beta'/\nu = 1.7$.

L/ξ . Additionally, f_+ is finite for $L < \xi$ but tends to zero for small $L^{-1}/|\Sigma - \Sigma_c|^\nu$, meaning that the number of MS packings vanishes for $\Sigma > \Sigma_c$ as L increases above ξ . If f_+ approaches a vertical asymptote, MS packings do not exist for $\Sigma > \Sigma_c$ and finite $L > \xi$. Otherwise, MS packings only vanish for infinite L . Further studies with larger system sizes are required to address this specific point. The inset to Fig. 2(b) shows $\langle \gamma_{\text{ms}}(\Sigma) \rangle^{-1}$, which is proportional to the density of MS packings, over a range of system sizes L , as well as the large-system limit implied by Eq. (1) and Fig. 2(b).

We show in Supplemental Material that the results for 2D systems with boundary driven simple shear are similar to those in 3D, with $\nu = 1.8 \pm 0.15$, $\Sigma_c = 0.11 \pm 0.01$, and $\beta/\nu \approx 0.57 \pm 0.06$. To verify that the scaling behavior is universal with respect to changes in the bound-

ary conditions and driving method, we show results from 2D systems of bidisperse frictionless grains in a riverbed-like geometry, similar to Ref. [17] and described in detail in Supplemental Material. The domain has a no-slip lower boundary at $y = 0$, a free upper boundary, and periodic horizontal boundaries in the x -direction with length L (in units of small grain diameters D). We use $N = 5L$ such that the system has height $H \approx 5D$. Particles interact via purely repulsive, linear springs with force constant K . We apply a buoyancy-reduced gravitational force $-mg'\hat{\mathbf{y}}$ and a horizontal fluid force $B(v_0 y_i/H \hat{\mathbf{x}} - \mathbf{v}_i)$ to each grain i , where B is a drag coefficient, y_i is the height above the lower boundary, v_0 is the characteristic velocity at the bed surface, and \mathbf{v}_i is the grain velocity. We find similar results for several different fluid flow profiles. We choose $\Gamma = \frac{B/m}{\sqrt{g'/D}} = 5$ and $\kappa = \frac{K}{mg'} = 1000$

and vary the dimensionless shear stress $\Sigma' = \frac{Bv_0}{mg'}$. Our results are again independent of κ and Γ in this regime.

We prepare beds via sedimentation with $\Sigma' = 0$ and then apply finite Σ' . We plot in Fig. 2(c) the ensemble-averaged distance $\langle \delta_{\text{ms}} \rangle$ traveled by a grain between the initial ($\Sigma' = 0$) and final ($\Sigma' > 0$) MS packings as a function of Σ' and L . Using a fitting analysis similar to the one discussed above for 3D boundary-driven simple shear, we identify $\Sigma'_c = 0.42 \pm 0.02$, $\beta'/\nu = 1.7 \pm 0.2$, and $\nu = 1.75 \pm 0.1$, suggesting that the scaling behavior and the value of $\nu \approx 1.8$ are generic with respect to changes in the spatial dimension, geometry, boundary conditions, and driving method.

To understand why the number of MS packings vanishes at Σ_c , we quantify the structure of MS packings generated via simple shear using the stress and contact fabric tensors [29, 30],

$$\sigma_{\alpha\lambda} = \frac{1}{V} \sum_{i \neq j} r_{\alpha}^{ij} F_{\lambda}^{ij} \quad (2)$$

$$R_{\alpha\lambda} = \frac{1}{N} \sum_{i \neq j} \frac{r_{\alpha}^{ij} r_{\lambda}^{ij}}{|\mathbf{r}^{ij}|^2}. \quad (3)$$

Here, α and λ are Cartesian coordinates, V is the system volume, r_{α}^{ij} is the α -component of the center-to-center separation vector between grains i and j , and F_{λ}^{ij} is the λ -component of the intergrain contact force. The sum over i and j includes all pairs of contacting particles (excluding grain-wall contacts).

Force balance requires $\sigma_{xy} = \sigma_{yx} = -\tau$, $\sigma_{yy} = p$, and $\sigma_{yz} = \sigma_{zy} = 0$, as shown in Fig. 3(c) and Supplemental Material. We also find $\sigma_{xz} = \sigma_{zx} = 0$ (Supplemental Material). Figure 3(d) shows that the force balance criterion $\sigma_{xy}/\sigma_{yy} = -\Sigma$ requires a proportional change in the corresponding fabric tensor component, $R_{xy}/R_{yy} = -a\Sigma$ with $a \approx 0.4$, meaning that grain-grain contacts are preferentially oriented along the compressive direction. Thus, the vanishing density of MS packings may be equivalent to an upper limit of the stress and corresponding fabric anisotropies that can be realized in a large system.

In Fig. 3(e) and (f), we show the excess normal stress $\sigma_{xx}/\sigma_{yy} - 1 \equiv \lambda_x$ and corresponding quantity from the fabric tensor $R_{xx}/R_{yy} - 1 \equiv \rho_x$. For $\Sigma < \Sigma_c$, λ_x and ρ_x begin at some finite value and tend to zero at large L . When $\lambda_x = 0$, the stress anisotropy $\Sigma_i \equiv \frac{\sigma_1 - \sigma_2}{\sigma_1 + \sigma_2} = \Sigma$, where $\sigma_{1,2}$ are the eigenvalues of the matrix with rows $(\sigma_{xx}, \sigma_{xy})$ and $(\sigma_{xy}, \sigma_{yy})$, which is decoupled from the z -direction of the stress tensor since $\sigma_{yz} = \sigma_{zy} = 0$ and $\sigma_{xz} = \sigma_{zx} = 0$. For $\Sigma > \Sigma_c$, λ_x and ρ_x increase with Σ . As shown in Supplemental Material, $\lambda_x > 0$ can give $\Sigma_i < \Sigma$, but this rotates the larger eigenvector σ_1 away from the compression direction by an angle θ' , where $\theta' \propto \lambda_x$ for small λ_x . (See Fig. 3(a).)

Near Σ_c for finite systems, MS packings are scarce, and $\Sigma_i < \Sigma$ with $\theta' > 0$ may be preferable, despite the broken

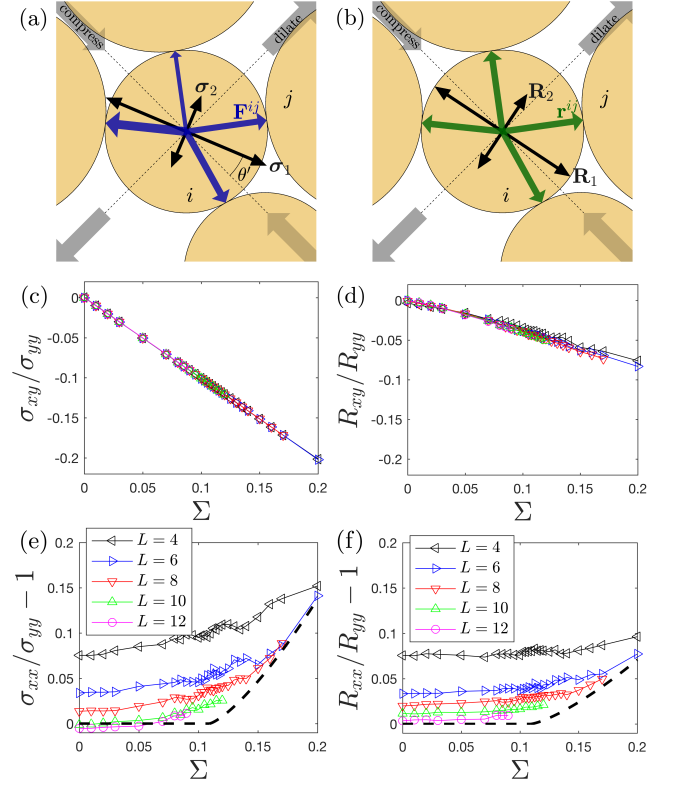


FIG. 3. (a,b) Close-up of MS packings in 2D illustrating features of the (a) stress and (b) fabric tensors for the central particle. $\sigma_{1,2}$ and $\mathbf{R}_{1,2}$ denote the eigenvalue-eigenvector pairs from the sum over the contacts (blue and green arrows) for the center grain i (Eqs. (2) and (3)). The magnitudes of the arrows are proportional to the eigenvalues and the directions are along the eigenvectors. θ' is the angle between the larger eigenvector and the compressive direction. (c,d) Ensemble averages of σ_{xy}/σ_{yy} and R_{xy}/R_{yy} for MS packings are plotted versus Σ for varying L , showing $\sigma_{xy}/\sigma_{yy} = -\Sigma$ and $R_{xy}/R_{yy} \approx -0.4\Sigma$ for all L . (e,f) Ensemble averages of the normal anisotropies in the (e) stress tensor, $\sigma_{xx}/\sigma_{yy} - 1 \equiv 2\lambda_x$, and (f) fabric tensor, $R_{xx}/R_{yy} - 1 \equiv 2\rho_x$, are plotted versus Σ for varying L . Dashed lines show the estimated large-system limit implied by the scaled data shown in Supplemental Material.

symmetry. However, the broken symmetry becomes more difficult to achieve for larger systems. We note that the dependence of λ_x and ρ_x on L in Fig. 3(e) and (f) is suggestive of critical scaling (which we expect if ξ dominates the behavior near Σ_c) similar to Eq. (1). We discuss the scaling behavior for λ_x and ρ_x (and the corresponding z -components) in the Supplemental Material.

In conclusion, for packings of frictionless spherical grains under shear, we find that the number of MS packings vanishes near $\Sigma = \Sigma_c \approx 0.11$ with corresponding critical scaling, shown in Fig. 2. This result, including the specific value of the exponent $\nu \approx 1.8$, is generic with respect to changes in spatial dimension, system geometry, and boundary conditions. The force balance crite-

rion, Fig. 3(c), is accompanied by a proportional change in the fabric tensor, Fig. 3(d). Thus, we argue that Σ_c corresponds to the maximum anisotropy that can be realized in the large-system limit. This hypothesis is consistent with our finding that finite-sized MS packings with Σ near or above Σ_c tend to be rotated relative to the axes of the applied deformation, which can reduce the internal force anisotropy of MS packings. However, this effect appears to vanish in the large-system limit, where symmetry dictates that compressive direction be aligned with the largest eigenvalues of the stress and fabric tensors for MS packings.

This research was sponsored by the Army Research Laboratory under Grant Numbers W911NF-14-1-0005 and W911NF-17-1-0164 (A.H.C., N.T.O., and C.S.O.). The views and conclusions contained in this document are those of the authors and should not be interpreted as representing the official policies, either expressed or implied, of the Army Research Laboratory or the U.S. Government. The U.S. Government is authorized to reproduce and distribute reprints for Government purposes notwithstanding any copyright notation herein. M.D.S. also acknowledges support from the National Science Foundation Grant No. CMMI-1463455.

-
- [1] F. da Cruz, S. Emam, M. Prochnow, J.-N. Roux, and F. Chevoir, "Rheophysics of dense granular materials: Discrete simulation of plane shear flows," *Phys. Rev. E* **72**, 021309 (2005).
 - [2] P. Jop, Y. Forterre, and O. Pouliquen, "A constitutive law for dense granular flows," *Nature* **441**, 727–730 (2006).
 - [3] B. S. Gardiner, B. Z. Dlugogorski, G. J. Jameson, and R. P. Chhabra, "Yield stress measurements of aqueous foams in the dry limit," *J. Rheol.* **42**, 1437–1450 (1998).
 - [4] A. S. Yoshimura, R. K. Prud'homme, H. M. Princen, and A. D. Kiss, "A comparison of techniques for measuring yield stresses," *J. Rheol.* **31**, 699–710 (1987).
 - [5] P. Coussot, Q. D. Nguyen, H. T. Huynh, and D. Bonn, "Avalanche behavior in yield stress fluids," *Phys. Rev. Lett.* **88**, 175501 (2002).
 - [6] A. Boromand, S. Jamali, and J. M. Maia, "Structural fingerprints of yielding mechanisms in attractive colloidal gels," *Soft matter* **13**, 458–473 (2017).
 - [7] Masahiro Toiya, Justin Stambaugh, and Wolfgang Losert, "Transient and oscillatory granular shear flow," *Phys. Rev. Lett.* **93**, 088001 (2004).
 - [8] N. Xu and C. S. O'Hern, "Measurements of the yield stress in frictionless granular systems," *Phys. Rev. E* **73**, 061303 (2006).
 - [9] P.-E. Peyneau and J.-N. Roux, "Frictionless bead packs have macroscopic friction, but no dilatancy," *Phys. Rev. E* **78**, 011307 (2008).
 - [10] C. S. O'Hern, L. E. Silbert, A. J. Liu, and S. R. Nagel, "Jamming at zero temperature and zero applied stress: The epitome of disorder," *Phys. Rev. E* **68**, 011306 (2003).
 - [11] A. Donev, S. Torquato, F. H. Stillinger, and R. Connelly, "Jamming in hard sphere and disk packings," *J. Appl. Phys.* **95**, 989–999 (2004).
 - [12] P. Olsson and S. Teitel, "Critical scaling of shear viscosity at the jamming transition," *Phys. Rev. Lett.* **99**, 178001 (2007).
 - [13] M. Van Hecke, "Jamming of soft particles: geometry, mechanics, scaling and isostaticity," *J. Phys. Condens. Matter* **22**, 033101 (2009).
 - [14] Brian P. Tighe, Erik Woldhuis, Joris J. C. Remmers, Wim van Saarloos, and Martin van Hecke, "Model for the scaling of stresses and fluctuations in flows near jamming," *Phys. Rev. Lett.* **105**, 088303 (2010).
 - [15] K. N. Nordstrom, E. Verneuil, P. E. Arratia, A. Basu, Z. Zhang, A. G. Yodh, J. P. Gollub, and D. J. Durian, "Microfluidic rheology of soft colloids above and below jamming," *Phys. Rev. Lett.* **105**, 175701 (2010).
 - [16] P. Olsson and S. Teitel, "Critical scaling of shearing rheology at the jamming transition of soft-core frictionless disks," *Phys. Rev. E* **83**, 030302 (2011).
 - [17] A. H. Clark, M. D. Shattuck, N. T. Ouellette, and C. S. O'Hern, "Onset and cessation of motion in hydrodynamically sheared granular beds," *Phys. Rev. E* **92**, 042202 (2015).
 - [18] A. H. Clark, M. D. Shattuck, N. T. Ouellette, and C. S. O'Hern, "Role of grain dynamics in determining the onset of sediment transport," *Phys. Rev. Fluids*, 034305 (2017).
 - [19] K. Kamrin and G. Koval, "Nonlocal constitutive relation for steady granular flow," *Phys. Rev. Lett.* **108**, 178301 (2012).
 - [20] M. Bouzid, M. Trulsson, P. Claudin, E. Clément, and B. Andreotti, "Nonlocal rheology of granular flows across yield conditions," *Phys. Rev. Lett.* **111**, 238301 (2013).
 - [21] D. L. Henann and K. Kamrin, "Continuum modeling of secondary rheology in dense granular materials," *Phys. Rev. Lett.* **113**, 178001 (2014).
 - [22] K. Kamrin and D. L. Henann, "Nonlocal modeling of granular flows down inclines," *Soft Matter* **11**, 179–185 (2015).
 - [23] M. Bouzid, A. Izzet, M. Trulsson, E. Clément, P. Claudin, and B. Andreotti, "Non-local rheology in dense granular flows," *Eur. Phys. J. E* **38**, 125 (2015).
 - [24] L. Bocquet, A. Colin, and A. Ajdari, "Kinetic theory of plastic flow in soft glassy materials," *Phys. Rev. Lett.* **103**, 036001 (2009).
 - [25] S. Karmakar, E. Lerner, and I. Procaccia, "Statistical physics of the yielding transition in amorphous solids," *Phys. Rev. E* **82**, 055103 (2010).
 - [26] J. Lin, E. Lerner, A. Rosso, and M. Wyart, "Scaling description of the yielding transition in soft amorphous solids at zero temperature," *Proc. Natl. Acad. Sci.* **111**, 14382–14387 (2014).
 - [27] N. Xu, C. S. O'Hern, and L. Kondic, "Velocity profiles in repulsive athermal systems under shear," *Phys. Rev. Lett.* **94**, 016001 (2005).
 - [28] T. Bertrand, R. P. Behringer, B. Chakraborty, C. S. O'Hern, and M. D. Shattuck, "Protocol dependence of the jamming transition," *Phys. Rev. E* **93**, 012901 (2016).
 - [29] D. Bi, J. Zhang, B. Chakraborty, and R. P. Behringer, "Jamming by shear," *Nature* **480**, 355–358 (2011).
 - [30] M. Baity-Jesi, C. P. Goodrich, A. J. Liu, S. R. Nagel, and J. P. Sethna, "Emergent $SO(3)$ symmetry of the frictionless shear jamming transition," *J. Stat. Phys.* **167**,

735–748 (2017).